Supporting Information

Cu(II)-Ln(III) (Ln = Gd, Tb and Dy) complexes of an unsymmetrical N_2O_3 donor ligand: Field induced SMM behaviour for Cu(II)-Tb(III) complex

Pradip Bhunia,[a] Souvik Maity,[a] Tanmoy Kumar Ghosh,[a] Arpan Mondal,[b] Júlia Mayans,[c] and Ashutosh Ghosh*[a]

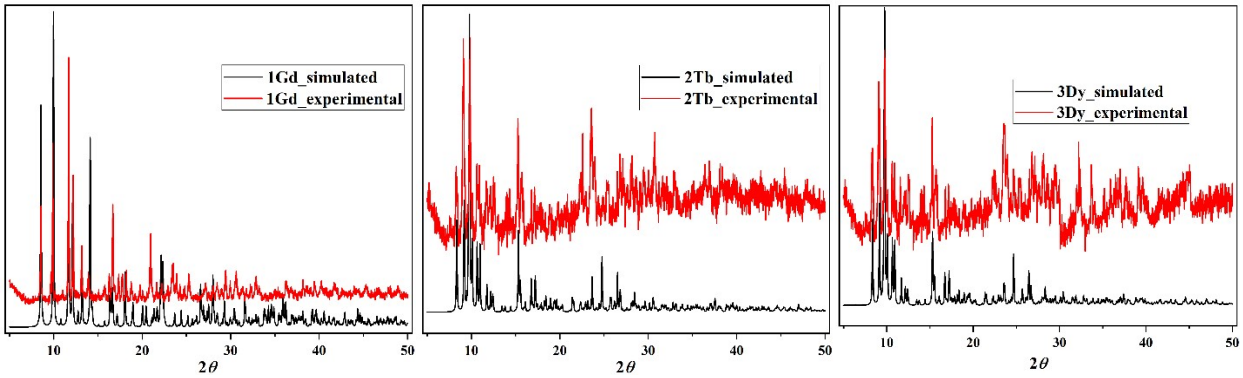

Fig. S1 Powder X-ray diffraction of Complexes **1** (left), **2** (middle) and **3** (right).

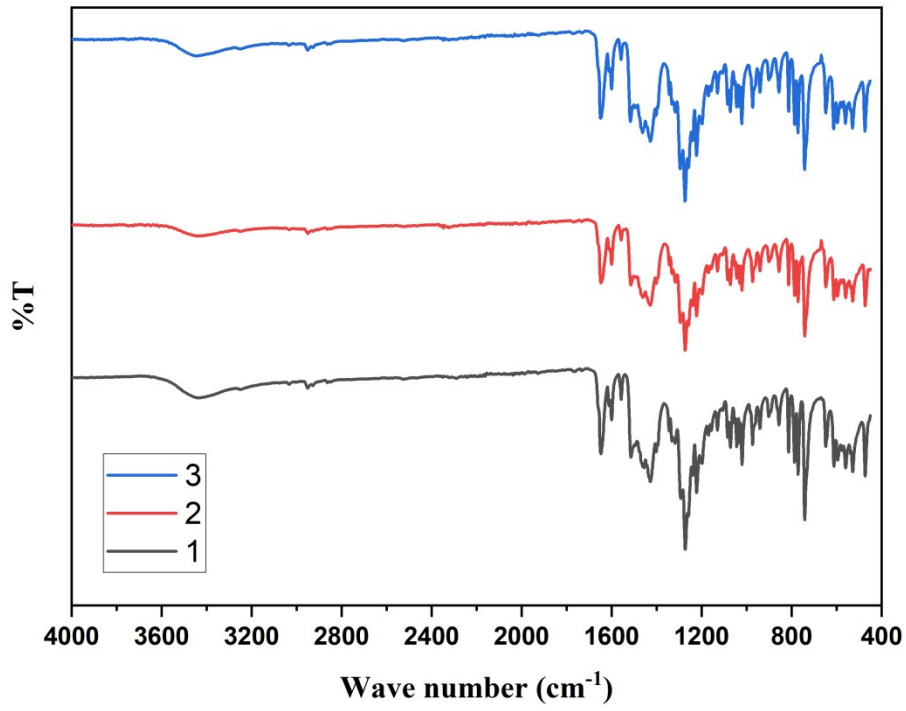

Fig. S2 IR spectra of complexes **1** — **3**.

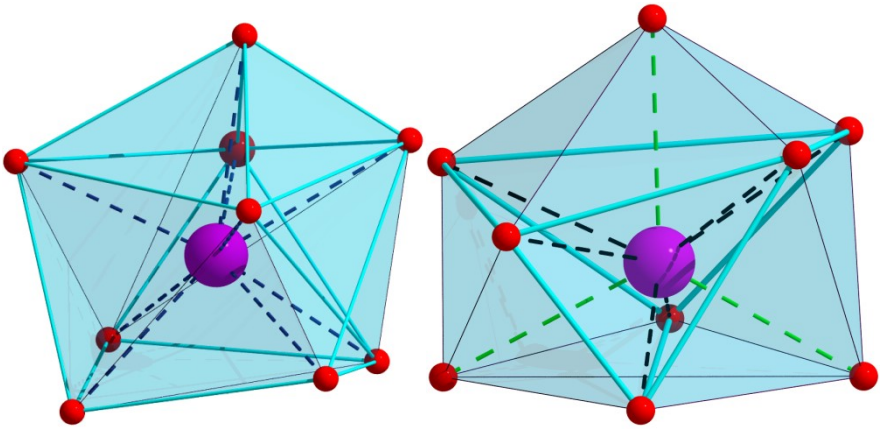

Fig. S3 Polyhedral view of Gd (**1**, left) and Ln (Tb(**2**) and Dy(**3**), right). (Colour code: Oxygen-red and violet- lanthanoid)

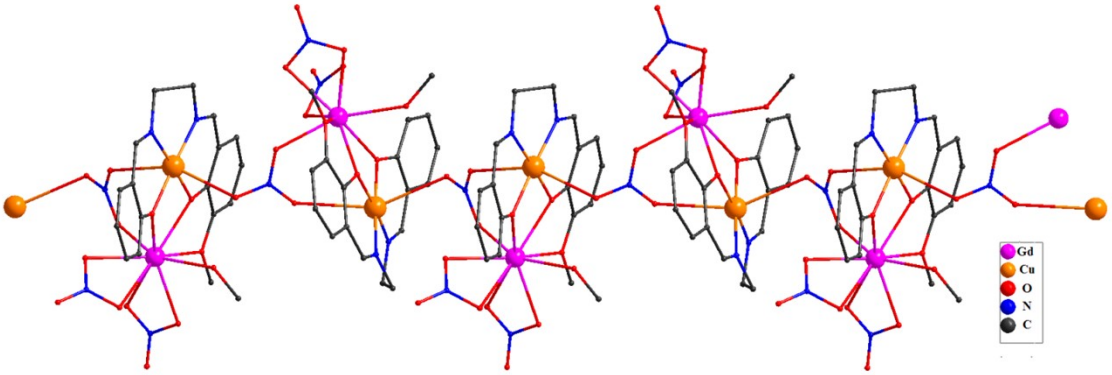

Fig. S4 Polymeric chain of complex **1.**

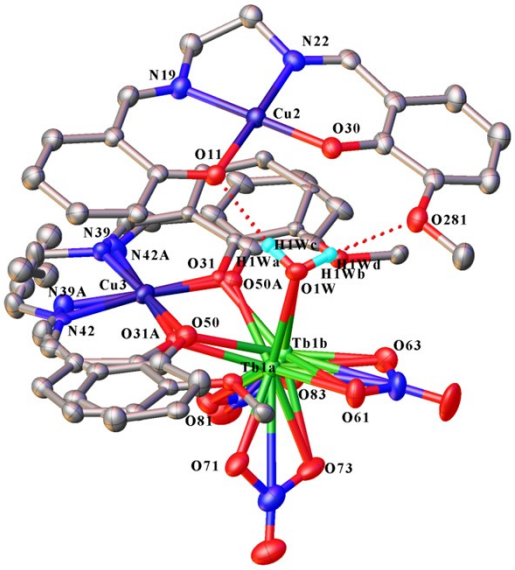

Fig. S5. ORTEP view of complex **2** with 20% ellipsoid probability. H-atoms except coordinated water molecules are omitted for clarity. H-bond presented by red dotted line.

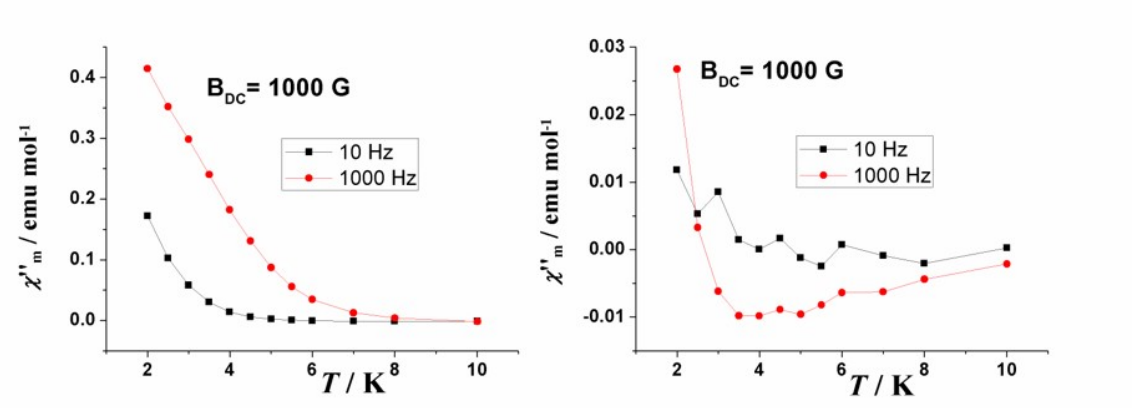

Fig. S6. DC field measurements for 1 (left) and 3 (right) indicating a non-clear response in their imaginary component of the susceptibility.

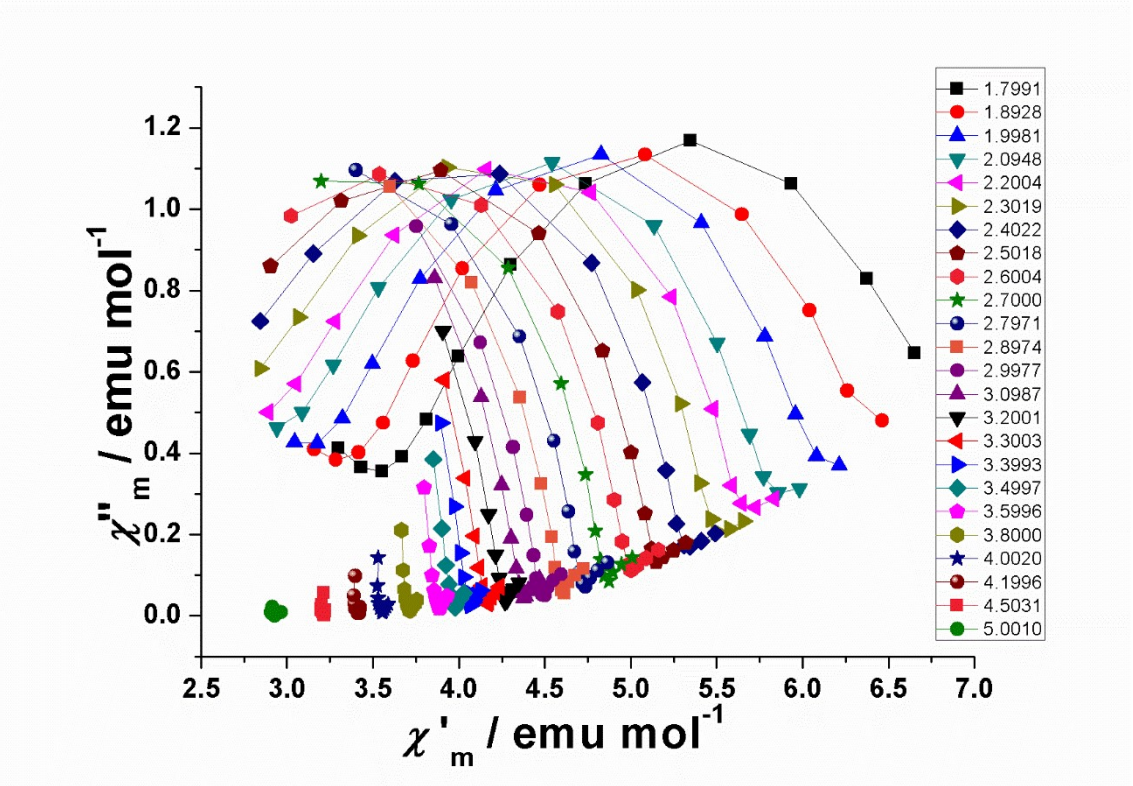

Fig. S7. χ' vs χ'' representation for complex **2**. Experimental data is represented with dots and the fitting with solid line.

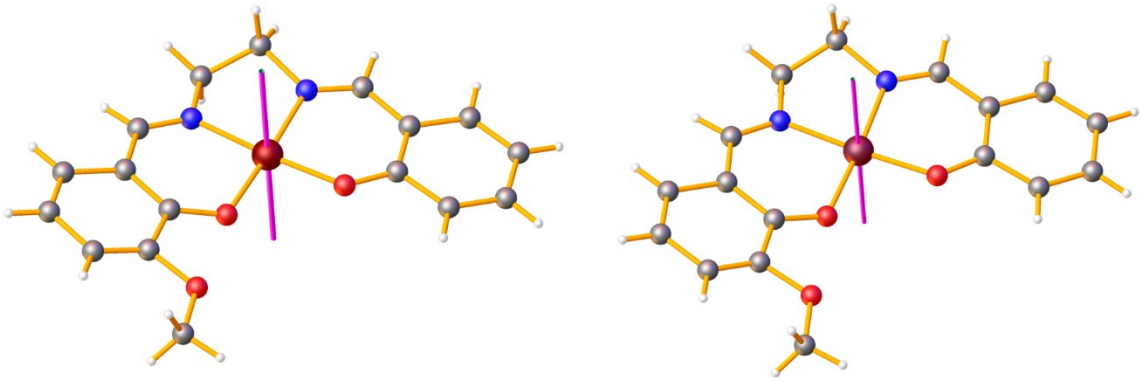

Fig. S8. The solid line corresponds to the orientation of main anisotropy axis in the ground state for Cu2 center in complex **2** (left) and **3** (right).

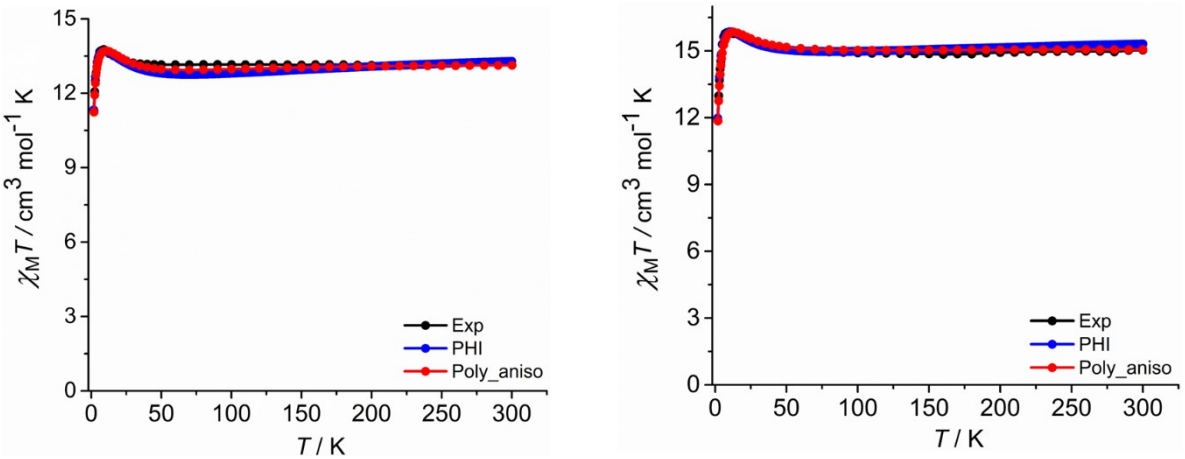

Fig. S9. Variable temperature magnetic susceptibility with the simulated susceptibility obtained form poly_aniso and PHI for complex **2** (left) and **3** (right).

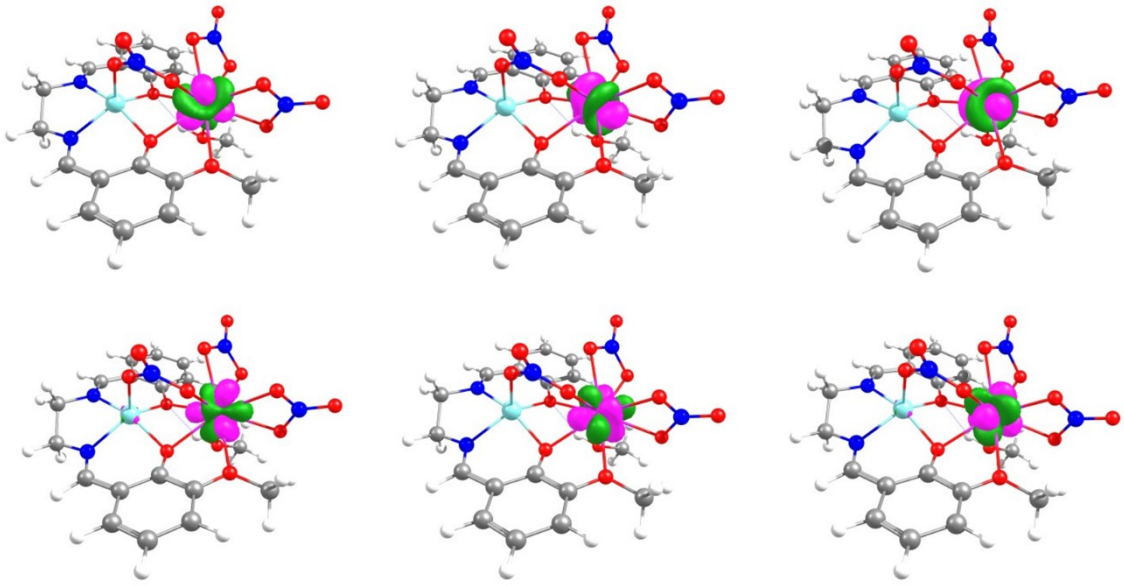

Fig. S10. Interacting 4f magnetic orbitals of Gd(III) center for complex **1**.

Table S1 SHAPE analysis for the lanthanoid canters in all complex (the lowest values are indicated in bold).

Geometry	Symmetry	**1**	**2**	**3**
Enneagon	D9h	34.280	33.956	30.559
Octagonal pyramid	C8v	21.594	18.597	17.487
Heptagonal bipyramid	D7h	14.346	18.461	18.590
Johnson triangular cupola J3	C3v	13.329	16.667	17.072
Capped cube J8	C4v	8.272	11.271	12.358
Spherical-relaxed capped cube	C4v	6.604	10.120	11.141
Capped square antiprism J10	C4v	3.408	3.896	5.317
Spherical capped square antiprism	C4v	**2.278**	3.266	4.569
Tricapped trigonal prism J51	D3h	4.233	5.405	7.142
Spherical tricapped trigonal prism	D3h	2.845	**2.698**	**4.506**
Tridiminished icosahedron J63	C3v	10.637	9.698	9.935
Hula-hoop	C2v	10.710	12.337	12.273
Muffin	Cs	2.922	4.294	5.012

Table S2 Bond lengths (Å) of complexes **1** – **3**.

Complex	**1**	Complex	**2 (M=Tb1b)**	**3 (M=Dy)**
Gd(1)-O(50)	2.332(3)	Dy(1)-O(50) M(1)-O(50A)	 2.51(2)	2.21(4) 2.39(2)
Gd(1)-O(1)	2.421(3)	M(1)-O(1W)	2.463(12)	2.401(9)
Gd(1)-O(61)	2.474(3)	M(1)-O(61)	2.402(14)	2.419(11)
Gd(1)-O(63)	2.456(3)	M(1)-O(81)	2.478(13)	2.466(10)
Gd(1)-O(31)	2.424(3)	M(1)-O(63)	2.558(15)	2.448(12)
Gd(1)-O(71)	2.489(3)	Dy(1)-O(31) M(1)-O(31A)	 2.26(2)	2.53(4) 2.327(19)
Gd(1)-O(73)	2.515(3)	M(1)-O(71)	2.320(17)	2.465(13)
Gd(1)-O(83)	2.401(3)	M(1)-O(73)	2.488(14)	2.509(11)

Gd(1)-O(481)	2.625(3)	M(1)-O(83)	2.638(17)	2.542(12)
Cu(3)-N(42)	1.922(3)	Cu(2)-O(30)	1.900(13)	1.908(9)
Cu(3)-O(50)	1.921(3)	Cu(2)-O(11)	1.906(12)	1.909(9)
Cu(3)-N(39)	1.919(3)	Cu(2)-N(22)	1.938(15)	1.937(11)
Cu(3)-O(31)	1.931(3)	Cu(2)-N(19)	1.935(16)	1.936(12)
Cu(3)-O(81)	2.787(4)	Cu(3)-N(42) Cu(3)-N(42A)	2.05(5) 1.98(3)	2.05(4) 2.01(2)
Cu(3)-O(84*)	2.729(3)	Cu(3)-O(50) Cu(3)-O(50A)	2.01(5) 2.00(2)	2.01(4) 1.99(2)
Gd(1)-N(62)	2.892(4)	Cu(3)-N(39) Cu(3)-N(39A)	1.73(5) 1.82(3)	1.73(4) 1.824(18)
Gd(1)-N(72)	2.935(4)	Cu(3)-O(31) Cu(3)-O(31A)	1.75(4) 1.84(2)	1.76(4) 1.849(18)

* = 1–x, -1/2+y, 1/2–z

Table S3 Bond angles (°) of complex **1**.

complex **1**			
O(1) -Gd(1)-O(31)	72.31(10)	O(63) - Gd(1)-O(71)	110.40(10)
O(1) - Gd(1)-O(50)	75.53(10)	O(63) - Gd(1)-O(73)	67.94(11)
O(1) - Gd(1)-O(61)	123.73(10)	O(63) - Gd(1)-O(83)	117.62(11)
O(1) - Gd(1)-O(63)	72.11(10)	O(63) - Gd(1)-O(481)	73.35(10)
O(1) - Gd(1)-O(71)	128.97(11)	O(71) - Gd(1)-O(73)	50.81(11)
O(1) - Gd(1)-O(73)	89.75(12)	O(71) - Gd(1)-O(83)	73.39(11)
O(1) - Gd(1)-O(83)	153.17(10)	O(71) - Gd(1)-O(481)	144.33(9)
O(1) - Gd(1)-O(481)	86.49(10)	O(73) - Gd(1)-O(83)	117.04(12)
O(31) - Gd(1)-O(50)	66.80(9)	O(73) - Gd(1)-O(481)	140.32(10)
O(31) - Gd (1)-O(61)	152.65(10)	O(81) - Gd(1)-O(481)	73.91(10)
O(31) - Gd(1)-O(63)	136.33(10)	O(31) -Cu(3)-N(39)	95.11(12)
O(31) - Gd(1)-O(71)	74.72(10)	O(31) -Cu(3)-N(42)	177.33(15)
O(31) - Gd(1)-O(73)	87.45(11)	O(31) -Cu(3)-O(50)	85.67(12)
O(31) - Gd(1)-O(83)	105.54(11)	O(31) -Cu(3)-O(81)	85.20(13)
O(31) - Gd(1)-O(481)	128.26(9)	O(31) -Cu(3)-O(84*)	77.04(10)
O(50) - Gd(1)-O(61)	135.04(10)	O(50) -Cu(3)-N(39)	174.77(15)

O(50) - Gd(1)-O(63)	125.82(10)	O(50) -Cu(3)-N(42)	94.55(14)
O(50) - Gd(1)-O(71)	123.75(10)	O(50) -Cu(3)-O(81)	83.55(11)
O(50) - Gd(1)-O(73)	153.09(10)	O(50) -Cu(3)-O(84*)	75.28(12)
O(50) - Gd(1)-O(83)	79.15(10)	O(81) -Cu(3)-N(39)	99.61(15)
O(50) - Gd(1)-O(481)	62.31(9)	O(81) -Cu(3)-N(42)	97.43(16)
O(61) - Gd(1)-O(63)	51.63(9)	O(81) -Cu(3)-O(84*)	153.29(12)
O(61) - Gd(1)-O(71)	78.31(11)	O(84*) -Cu(3)-N(39)	101.68(14)
O(61) - Gd(1)-O(73)	71.86(11)	O(84*) -Cu(3)-N(42)	100.34(14)
O(61) - Gd(1)-O(83)	70.38(10)	N(39) -Cu(3)-N(42)	84.92(14)
O(61) - Gd(1)-O(481)	77.67(10)	* = 1–x, -1/2+y, 1/2–z	

Table S4 Bond angles (°) of complexes **2** – **3**.

Complex	**2** **(M= Tb)**	**3** **(M =Dy)**		**2** **(M = Tb)**	**3** **(M= Dy)**
O(1w) -M(1)-O(31)	82.9(7)	82.2(5)	O(61) -M(1)-O(81)	145.0(5)	143.3(4)
O(1w) -M(1)-O(50)	70.7(8)	73.0(7)	O(61) -M(1)-O(83)	115.1(5)	118.4(4)
O(1w) -M(1)-O(61)	75.7(5)	75.4(4)	O(63) -M(1)-O(71)	115.4(5)	114.7(4)
O(1w) -M(1)-O(63)	78.3(5)	80.5(4)	O(63) -M(1)-O(73)	70.5(6)	72.1(4)
O(1w) -M(1)-O(71)	137.0(5)	130.7(3)	O(63) -M(1)-O(81)	116.2(5)	121.5(4)
O(1w) -M(1)-O(73)	145.1(5)	145.5(4)	O(63) -M(1)-O(83)	69.9(5)	73.5(4)
O(1w) -M(1)-O(81)	137.8(4)	141.3(3)	O(71) -M(1)-O(73)	52.2(6)	50.7(4)
O(1w) -M(1)-O(83)	118.2(5)	124.7(4)	O(71) -M(1)-O(81)	75.2(5)	72.5(4)
O(31A) -M(1)-O(50A)	67.5(7)	65.5(3)	O(71) -M(1)-O(83)	104.6(5)	104.6(4)
O(31A) -M(1)-O(61)	130.0(6)	123.5(5)	O(73) -M(1)-O(81)	72.4(5)	72.7(4)
O(31A) -M(1)-O(63)	160.2(7)	162.7(6)	O(73) -M(1)-O(83)	65.0(6)	67.0(4)
O(31A) -M(1)-O(71)	82.8(7)	77.2(5)	O(81) -M(1)-O(83)	47.6(5)	50.1(4)
O(31A) -M(1)-O(73)	129.2(8)	124.0(6)	O(11) -Cu(2)-N(19)	92.3(6)	93.2(5)
O(31A) -M(1)-O(81)	74.6(7)	73.1(5)	O(11) -Cu(2)-N(22)	176.3(6)	176.6(4)
O(31A) -M(1)-O(83)	114.9(6)	117.0(5)	O(11) -Cu(2)-O(30)	89.6(5)	89.7(4)
O(50A) -M(1)-O(61)	139.9(8)	144.5(7)	O(30) -Cu(2)-N(19)	176.8(6)	176.4(4)
O(50A) -M(1)-O(63)	101.0(7)	106.9(6)	O(30) -Cu(2)-N(22)	93.1(6)	92.3(5)
O(50A) -M(1)-O(71)	136.7(7)	134.3(6)	N(19) -Cu(2)-N(22)	85.0(7)	84.7(5)

O(50A) -M(1)-O(73)	129.7(8)	134.6(7)	O(31) -Cu(3)-N(39) O(31A) -Cu(3)-N(39A)	103.0(16) 99.0(10)	103.6(16) 99.3(8)
O(50A) -M(1)-O(81)	67.7(8)	70.2(7)	O(31) -Cu(3)-N(42) O(31A) -Cu(3)-N(42A)	174.5(15) 175.0(13)	172.8(15) 176.1(11)
O(50A) -M(1)-O(83)	65.6(7)	69.4(7)	O(31) -Cu(3)-O(50) O(31A) -Cu(3)-O(50A)	83.5(16) 86.2(9)	83.2(15) 86.0(8)
O(61) -M(1)-O(63)	50.3(5)	51.5(4)	O(50) -Cu(3)-N(39) O(50A) -Cu(3)-N(39A)	170.0(2) 173.4(12)	172.2(15) 173.4(9)
O(61) -M(1)-O(71)	83.3(5)	79.6(4)	O(50) -Cu(3)-N(42) O(50A) -Cu(3)-N(42A)	91.2(16) 92.1(10)	89.9(13) 91.6(9)
O(61) -M(1)-O(73)	72.6(2)	71.3(4)	N(39) -Cu(3)-N(42) N(39A) -Cu(3)-N(42A)	82.5(16) 82.4(11)	83.5(13) 82.8(9)

Table S5. Geometrical features of hydrogen bonding interactions (distances (Å) and angles (°)) of Complexes **2** and **3.**

Complex	D−H···A	D−H (Å)	H···A (Å)	D···A (Å)	∠D−H···A (°)
1	O(1) –H(1) ···O(84*)	0.85(3)	1.95(3)	2.796(4)	174.7(7)
2	O(1W) –H(1WC) ···O(11)	0.861(18)	1.945(18)	2.791(18)	167.3(13)
	O(1W) –H(1WD) ···O(281)	0.860(16)	2.163(18)	2.894(18)	142.7(13)
3	O(1W) –H(1WB) ···O(11)	0.86(3)	1.96(3)	2.793(12)	165(4)
	O(1W) –H(1WA) ···O(281)	0.87(6)	2.18(5)	2.908(14)	142(7)

* = 1–x, -1/2+y, 1/2–z

Table S6: Main values of the g tensor for the lowest Kramers doublet on **Cu1** site in complex **2** and **3**.

Complex	Energy (cm^{-1})	g_x	g_y	g_z	Average g
2	0.000	2.068	2.078	2.358	2.168
3	0.000	2.071	2.079	2.371	2.173

Table S7: Main values of the g tensor for the lowest Kramers doublet on **Cu2** site in complex **2** and **3**.

Complex	Energy (cm^{-1})	g_x	g_y	g_z	Average g

2	0.000	2.075	2.079	2.429	2.194
3	0.000	2.071	2.079	2.434	2.194

Table S8. Ab initio calculated low-lying spin-free energy states for the complexes **2** and **3**.

Complex 2			**Complex 3**		
Tb1	**Cu1**	**Cu2**	**Dy1**	**Cu1**	**Cu2**
0.000	0.000	0.000	0.000	0.000	0.000
254.1866	15104.0	12832.9	5.1881	14616.6	12681.9
334.7954	16435.3	15168.2	146.0808	15916.8	15071.1
589.7838	17186.4	15920.1	189.2308	16759.6	15760.1
681.7127	17396.5	16359.1	311.2849	16888.2	16206.1
841.1414			389.2209		
1047.7667			404.9580		
25752.8283			457.5970		
25772.8797			522.1624		
25860.9570			767.0082		

Table S9. Ab initio calculated low-lying spin-orbit energy states for the investigated complexes.

Complex 2			**Complex 3**		
Tb1	**Cu1**	**Cu2**	**Dy1**	**Cu1**	**Cu2**
0.0000	0.0000	0.0000	0.000	0.000	0.000
0.1382	0.0000	0.0000	0.000	0.000	0.000
166.8520	14967.2421	12795.27	121.8143	14481.71	12648.00
172.6762	14967.2421	12795.27	121.8143	14481.71	12648.00
248.0922	16220.40	15041.99	253.3184	15718.18	14928.88
273.0234	16220.40	15041.99	253.3184	15718.18	14928.88
339.0670	16871.93	15548.70	309.6681	16405.01	15398.94
384.8721	16871.93	15548.70	309.6681	16405.01	15398.94
411.9902	18363.77	17244.88	331.8373	17887.30	17097.81
523.7558	18363.77	17244.88	331.8373	17887.30	17097.81
			388.2979		
			388.2979		
			488.8733		
			488.8733		
			668.6695		
			668.6695		

Table S10. CASSCF/QDPT/Single_aniso computed energy of the KDs, g, and wave functions composition for first four low-lying states in complex **2** (Tb1).

State	Energy (cm^{-1})	Tunnel Splitting	g_z	Wave function composition
1	0.000	0.138	17.86	99.53%|±6>+0.27%|±4
2	0.138			99.59%|±6>+0.26%|±4
3	166.852	5.824	14.33	80.59%|±5+3.93%|±4+7.56%|±3+5.18%|±2+0.94%|±1
4	172.676			85.48%|±5+4.49%|±4+5.79%|±3+3.22%|±2+0.95%|±1

Table S11. CASSCF/QDPT/Single_aniso computed energy of the KDs, g, and wave functions composition in complex **3** (Dy1).

Kramers doublets (KDs)	Energy (cm^{-1})	g_x	g_y	g_z	Wave function composition
1	0.000	0.07	0.010	19.59	95.82%|±15/2>+0.04%|±13/2>+3.26%|±11/2>
2	121.814	0.021	0.024	17.02	0.40%|±15/2>+90.66%|±13/2>+5.53%|±11/2>+1.65%|±9/2>+0.95%|±5/2>
3	253.318	1.280	1.783	12.98	2.82%|±15/2>+3.58%|±13/2>+65.69%|±11/2>+12.81%|±9/2>+9.21%|±7/2>+1.30%|±5/2>+1.39%|±3/2>+3.14%|±1/2>
4	309.668	1.444	2.442	13.82	0.12%|±15/2>+1.10%|±13/2>+6.43%|±11/2>+23.90%|±9/2>+14.26%|±7/2>+36.01%|±5/2>+13.47%|±3/2>+4.66%|±1/2>
5	331.837	2.436	4.408	12.89	0.27%|±15/2>+0.96%|±13/2>+1.37%|±11/2>+10.22%|±9/2>+10.01%|±7/2>+7.64%|±

					5/2>+33.93%|±3/2>+35.56%|±1/2>
6	388.298	0.879	1.872	15.88	0.31%|±15/2>+3.01%|±13/2>+14.98%|±11/2>+36.36%|±9/2>+27.77%|±7/2>+9.56%|±5/2>+6.73%|±3/2>+1.25%|±1/2>
7	488.873	0.089	0.118	16.35	0.13%|±15/2>+0.15%|±13/2>+1.94%|±11/2>+12.49%|±9/2>+25.08%|±7/2>+13.35%|±5/2>+11.54%|±3/2>+35.28%|±1/2>
8	668.669	0.007	0.014	18.94	0.08%|±15/2>+0.46%|±13/2>+0.75%|±11/2>+2.31%|±9/2>+13.08%|±7/2>+31.07%|±5/2>+32.34%|±3/2>+19.87%|±1/2>

Table S12. SINGLE_ANISO computed crystal-field parameters for the lanthanide center in complexes **1** and **2**.

		Complex 2	**Complex 3**
K	q	**Tb1**	**Dy1**
	-2	-0.5261E+01	0.1574E+01
	-1	-0.6857E+00	0.5950E+00
2	0	-0.4754E+01	-0.2714E+01
	1	-0.1734E+01	0.1012E+01
	2	-0.6196E-02	0.1588E+01
	-4	-0.6018E-03	0.2508E-03
	-3	0.2929E-01	-0.4772E-02
	-2	0.1686E-01	-0.4153E-02
	-1	0.4202E-02	-0.1043E-01
4	0	-0.5043E-02	-0.2099E-02
	1	0.2964E-01	-0.2939E-01
	2	0.6283E-02	-0.8008E-03
	3	0.1402E-00	-0.2539E-01
	4	-0.3491E-03	-0.5173E-02

	-6	-0.4128E-03	-0.1019E-03
	-5	-0.6881E-03	-0.1055E-02
	-4	-0.1172E-03	-0.9520E-04
	-3	-0.1959E-03	-0.1700E-03
	-2	0.2133E-03	-0.1581E-03
	-1	0.2354E-03	0.1474E-03
6	0	0.3132E-04	0.1186E-04
	1	-0.3867E-03	0.4096E-03
	2	-0.2158E-03	0.1536E-03
	3	-0.6206E-03	-0.3542E-04
	4	-0.2341E-03	-0.1681E-03
	5	0.1029E-02	-0.1925E-03
	6	0.4778E-03	0.1193E-03

The following Hamiltonian is used to calculate the crystal field parameters.

$$\hat{H}_{CF} = \sum_{k=-q}^{q} B_q^k \hat{o}_q^k$$

Where $\hat{o}_q^k$ =extended stevens operator, k = rank of the ITO (2,4,6), q = the component of the ITO, = -k, -k+1, ... 0, 1, ... k.

Simulation of molar magnetic susceptibility

To quantify, the exchange interaction, we have performed the simulations of molar magnetic susceptibilitydatausing PHI software[9] and Poly_aniso module[10] of ORCA 5.0.2 for the studied complexes. In PHI, we have used the following Hamiltonian (Eq-a) wherethe crystal field parameters obtained from the ab initio calculations were kept fixed during the simulation (here J_1 and $J_2 = J_{total} = J_{dip} + J_{ex}$).

$$\hat{H}_{CF} = -2J_1 (S_{Cu1} \cdot S_{Ln1}) - 2J_2 (S_{Cu2} \cdot S_{Ln1}) + \beta(g_{Cu1} \cdot S_{Cu1} + g_{Cu2} \cdot S_{Cu2} + g_{Ln1} \cdot S_{Ln1}) \cdot B + B_0^2 C_0^2 + B_0^4 C_0^4 + B_0^6 C_0^6 \ldots\ldots\ldots \text{(Eq-a)}$$

The best simulation of both susceptibility and magnetization results in ferromagnetic interactions between Cu and lanthanide metal ions (Table S13) with the intermolecular interactions of -0.011 and -0.013 cm^{-1} for complexes **2** and **3** respectively.

Further, the simulation was also performed using poly_aniso with Ising-type Hamiltonian (Eq-b) and intermolecular interactions.

$$\hat{H} = -J_1(\hat{S}_{Cu1,z}.\hat{S}_{Ln1,z}) - J_2(\hat{S}_{Cu2,z}.\hat{S}_{Ln1,z}) + zJ \ldots\ldots\ldots\ldots \text{(Eq-b)}$$

The dipolar part is considered exactly (Table S14) while the exchange part was obtained from the best fitting of the susceptibility data (Table S13). The best simulation of magnetic data results in ferromagnetic interactions between Cu and lanthanide metal ions for the studied complexes.

Table S13: Parameters obtained from the simulation of magnetic data using PHI and Poly_aniso module for complexes **2** and **3**.

	PHI					Poly_aniso		
Complex	J_1 **(cm^{-1})**	J_2 **(cm^{-1})**	g_{Cu}	g_{Ln}	**CF parameter / cm^{-1}**	J_1 **(cm^{-1})**	J_2 **(cm^{-1})**	zJ **(cm^{-1})**
2	+15.5	+3.5	2.17	1.48 (g_J)	$B^0_{2=}$ -4.754 $B^0_{4=}$ -0.00504 $B^0_{6=}$ 3.13 × 10^{-5}	+9.02	+1.8	-0.040
3	+16.3	+5.9	2.16	1.30 (g_J)	$B^0_{2=}$ –2.714 $B^0_{4=}$ – 0.0020 $B^0_{6=}$ 1.18 × 10^{-5}	+12.03	+3.8	-0.063

Table S14: Poly_aniso calculated energy of the lowest spin-orbit states (cm^{-1}) for complexes **2** and **3**.

Complex 2				Complex 3			
Exchange only	**Dipole-dipole**	**Total**	**Total relative**	**Exchange only**	**Dipole-dipole**	**Total**	**Total relative**
-15.869	-0.17780	-16.011	0.00000	-19.368	-0.26404	-19.536	0.0000
-15.869	-0.17288	-16.011	0.00015	-19.368	-0.26404	-19.536	0.0000
-10.578	-0.10099	-10.709	5.30251	-10.298	-0.19208	-10.492	9.0435
-10.576	-0.09893	-10.707	5.30429	-10.298	-0.19208	-10.492	9.0435
10.275	0.22907	10.400	26.4126	9.575	0.19058	9.7663	29.302
10.277	0.23026	10.402	26.4139	9.575	0.19058	9.7663	29.302
15.560	0.31900	15.716	31.7281	18.633	0.26543	18.817	38.354
15.567	0.32493	15.722	31.7344	18.633	0.26543	18.817	38.354
157.312	166.835	157.150	173.162	105.841	121.600	105.743	125.280
157.316	166.837	157.155	173.167	105.841	121.600	105.743	125.280
161.277	166.847	161.115	177.127	113.652	121.657	113.515	133.051
161.330	166.867	161.163	177.175	113.652	121.657	113.515	133.051

178.633	172.669	178.786	194.798	130.701	121.971	130.824	150.360
178.682	172.670	178.830	194.842	130.701	121.971	130.824	150.360
182.661	172.682	182.827	198.839	138.518	122.028	138.618	158.155
182.664	172.703	182.833	198.845	138.518	122.028	138.618	158.155

Table S15. Energies (cm^{-1}) of the low-lying exchange doublet states for the complexes **2** and **3**.

Complex 2		**Complex 3**	
Energy	g_z	Energy	g_z
0.00000 0.00015	22.29	0.00000 0.00000	23.89
5.302 5.304	17.81	9.044 9.044	19.57

Ab initio calculations details

All calculations were carried out on the coordinates obtained from the relevant crystal structure using the ORCA 5.0.2 software package.[1] The position of hydrogen atoms was optimized at the DFT level using pure GGA PBE exchange correlation functional[2] keeping constant the position of other atoms. To avoid the convergence problem, we have used diamagnetic Y^{+3} ion during the optimizations. The def2-TZVP basis sets with effective core potential (ECP) to treat the core electrons of Y have been used throughout DFT the calculations. The DKH Hamiltonian was used throughout to consider relativistic effects. The lanthanide centre was modelled with the SARC2-DKH-QZVP basis set, and all other atoms were treated with the DKH-def2-TZVP basis set in combination with the 'AutoAux' auxiliary basis set.[3] The active space was constructed from nine electrons in five d orbitals CAS(9,5) for Cu(II) ions,, eight electrons in seven f-orbitals for terbium CAS(8,7) and CAS(9,7) was constructed from nine electrons in seven f-orbitals for dysprosium.In the configuration integration procedure we have computed 5 doublet excited states for each of the Cu(II) ion to extract the spin projection on respective Cu(II) ions in complexes **2** and **3** while 7 septets, 76 quintets, and 52 triplets for terbium and 21 sextets, 128 quartets, and 130 doublets were considered for dysprosium. To include the spin-orbit coupling, we also used the quasi-degenerate perturbation theory (QDPT) approach using SA-CASSCF wave functions.[4] The SINGLE_ANISO module as implemented in ORCA was used to compute the *g*-tensor and crystal field parameters of the low-lying excited states using previously calculated spin-orbit states.[5] Further, to estimate the Cu-Ln exchange interactions and analyse possible relaxation dynamics we have used Poly_aniso module for the simulation of magnetic susceptibility data.

DFT calculations details

The BS-DFT calculations were performed on the coordinates obtained from the X-ray structure using Gaussian09[5] programme without optimizations. We used hybrid B3LYP functional along

with effective core potential 'Stuttgart RSC 1997' basis set[6] for Gd, and Ahlrichs triple-ζ TZV basis set[7] for the other atoms. The exchange coupling constants have been calculated by Yamaguchi approach as it is approximately valid over the whole coupling strength regime using equation 1, where E_T, E_{BS}, and S represent the energy of the high spin state, broken-symmetry state and total spin respectively.

$$J = \frac{-(E_T - E_{BSS})}{\langle S^2 \rangle_T - \langle S^2 \rangle_{BSS}} \quad \text{.....Eq. c}$$

Energy of the high spin and broken symmetry state for **1**			
Spin State	Energy (Hatree)	$\langle S^2 \rangle$	J (cm^{-1})
HS	-4356.11443701	20.01	+2.93
BS	-4356.11434342	13.01	

Reference

1. F. Neese, F. Wennmohs, U. Becker and C. Riplinger, *J. chem. phys.*, 2020, **152**, 224108.
2. (a) J. P. Perdew, K. Burke and M. Ernzerhof, Phys. Rev. Lett., 1997, 78, 1396-1396; (b) J. P. Perdew, K. Burke and M. Ernzerhof, Phys. Rev. Lett., 1996, 77, 3865-3868.
3. (*a*) D. Aravena, F. Neese and D. A. Pantazis, *J. Chem. Theory Comput.*, 2016, **12**, 1148-1156; (*b*) J. Chmela and M. E. Harding, *Mol. Phys.*, 2018, **116**, 1523-1538; (*c*) F. Weigend and R. Ahlrichs, *Phys. Chem. Chem. Phys.*, 2005, **7**, 3297-3305.
4. D. Ganyushin and F. Neese, *J. Chem. Phys.*, 2006, **125**, 24103.
5. L. F. Chibotaru and L. Ungur, *J. Chem. Phys.*, 2012, **137**, 64112.
6. M. J. Frisch, G. W. Trucks, H. B. Schlegel, G. E. Scuseria, M. A. Robb, J. R. Cheeseman, G. Scalmani, V. Barone, G. A. Petersson, H. Nakatsuji, X. Li, M. Caricato, A. V. Marenich, J. Bloino, B. G. Janesko, R. Gomperts, B. Mennucci, H. P. Hratchian, J. V. Ortiz, A. F. Izmaylov, J. L. Sonnenberg, Williams, F. Ding, F. Lipparini, F. Egidi, J. Goings, B. Peng, A. Petrone, T. Henderson, D. Ranasinghe, V. G. Zakrzewski, J. Gao, N. Rega, G. Zheng, W. Liang, M. Hada, M. Ehara, K. Toyota, R. Fukuda, J. Hasegawa, M. Ishida, T. Nakajima, Y. Honda, O. Kitao, H. Nakai, T. Vreven, K. Throssell, J. A. Montgomery Jr., J. E. Peralta, F. Ogliaro, M. J. Bearpark, J. J. Heyd, E. N. Brothers, K. N. Kudin, V. N. Staroverov, T. A. Keith, R. Kobayashi, J. Normand, K. Raghavachari, A. P. Rendell, J. C. Burant, S. S. Iyengar, J. Tomasi, M. Cossi, J. M. Millam, M. Klene, C. Adamo, R. Cammi, J. W. Ochterski, R. L. Martin, K. Morokuma, O. Farkas, J. B. Foresman and D. J. Fox, *Journal*, 2016.
7. M. Dolg, H. Stoll and H. Preuss, *J. Chem. Phys.*, 1989, **90**, 1730-1734.
8. A. Schäfer, C. Huber and R. Ahlrichs, *J. Chem. Phys*., 1994, **100**, 5829-5835.